Scale Sensitivity of the Gill Circulation. Part II: Off-Equatorial Case

Gilles Bellon, Beatriz Reboredo

Scale Sensitivity of the Gill Circulation. Part II: Off-Equatorial Case

GILLES BELLON[a,b] AND BEATRIZ REBOREDO[a]

[a] *Department of Physics, University of Auckland, Auckland, New Zealand*
[b] *Centre National de Recherches Météorologiques, Université de Toulouse, Météo France, CNRS, Toulouse, France*

(Manuscript received 10 March 2021, in final form 25 August 2021)

ABSTRACT: We investigate the steady dynamical response of the atmosphere on the equatorial β plane to a steady, localized, midtropospheric heating source. Following Part I, which investigates the case of an equatorial diabatic heating, we explore the sensitivity of the Gill circulation to the latitudinal location of the heating, together with the sensitivity to its horizontal scale. Again, we focus on characteristics of the response that would be particularly important if the circulation interacted with the hydrologic and energy cycles: overturning circulation and low-level wind. In the off-equatorial case, the intensity of the overturning circulation has the same limit as in the equatorial case for small horizontal extent of the diabatic heating, which is also the limit in the *f*-plane case. The decrease in this intensity with increasing horizontal scale of the diabatic heating is slightly faster in the off-equatorial case than in the equatorial case, which is due to the increase of rotational winds at the expense of divergent winds. The low-level westerly jet is more intense than in the equatorial case, with larger maximum wind and eastward mass transport that tend to infinity for small horizontal extent of the diabatic heating. In terms of spatial characteristics, this jet has a similar latitudinal extent as in the equatorial case but, unlike in the equatorial case, it extends farther equatorward than poleward of the diabatic-heating center. It also extends farther eastward than in the equatorial case.

KEYWORDS: Atmosphere; Atmospheric circulation; Idealized models; Large-scale motions; Monsoons; Shallow-water equations; Tropics

1. Introduction

Gill's (1980, hereafter G80) seminal work showed that the damped, linear, baroclinic dynamical response of the tropical atmosphere to a localized, steady, midtropospheric diabatic heating reproduces the main features of some tropical circulations. G80's study aimed to provide a very simple model of the Walker circulation resulting from equatorial regional diabatic heating, a success with some caveats as pointed in Reboredo and Bellon (2021, hereafter Part I), as well as of the monsoon circulations resulting from off-equatorial diabatic heating (Webster 1972). Monsoon circulations exhibit distinct features compared to circulations in response to equatorial forcing, and in particular a change of direction of off-equatorial low-level winds from easterlies to westerlies to form a monsoon jet (Ramage 1971; Joseph and Raman 1966).

In the context of slow intraseasonal oscillations (30–60 days), for which the circulation can be considered in quasi equilibrium with the diabatic heating, the off-equatorial Gill circulation is particularly relevant to the monsoon intraseasonal oscillation [also called northward-propagating, boreal-summer intraseasonal oscillation; see Goswami (2005) for a review]. Although the main mechanisms of this intraseasonal oscillation are still debated (Jiang et al. 2004; Bellon and Srinivasan 2006; Bellon and Sobel 2008a; Boos and Kuang 2010; Kang et al. 2010; Sharmila et al.2013; Gao et al. 2019), moisture-convergence feedback and wind-induced surface heat fluxes are expected to play major roles in the development and propagation of the convective disturbances. A better theoretical understanding of the off-equatorial Gill circulation is therefore useful to improve our grasp of the dynamical features susceptible to impact these feedbacks.

G80 focused on two cases: the simplest case with diabatic heating symmetric about the equator and the simplest case with diabatic heating antisymmetric about the equator. G80 considered that the monsoon circulation was well represented by the sum of these two solutions, but monsoon circulations are probably better depicted by the dynamical response of the tropical atmosphere to a simple patch of off-equatorial diabatic heating rather than by the response to the sum of these two heating patterns (Wu et al. 2009), and extending G80's work to study this response is the motivation of this article. We base a lot of the present work on the derivations presented in Part I, in which we analyze the scale dependence of the equatorial Gill circulation.

In section 2, we present some specifics of the off-equatorial case to complete the derivations in Part I. Section 3 presents some solutions as well as the scale sensitivity of the overturning circulation and of the low-level wind to the size and latitude of the imposed diabatic heating. Section 4 summarizes our findings and concludes. As in Part I, for brevity, we will refer to "imposed diabatic heating" simply as "heating" in the next sections.

2. Method

a. Semianalytical solutions

We use the analytical results of Part I (sections 2a and 2b) that we summarize briefly here. We use the Matsuno–Gill equations (Matsuno 1966; G80; Part I):

$$\varepsilon u - \frac{1}{2} y v = -\partial_x T, \tag{1}$$

Publisher's Note: This article was revised on 24 March 2022 to fix Figs. 3, 5, 6, and 7, whose original formatting was not consistent with the rest of the figures when originally published.

Corresponding author: Gilles Bellon, gilles.bellon@auckland.ac.nz

DOI: 10.1175/JAS-D-21-0068.1

$$\frac{1}{2}yu = -\partial_y T, \tag{2}$$

$$\varepsilon T + \partial_x u + \partial_y v = Q, \tag{3}$$

with (u, v) the horizontal baroclinic velocity (i.e., the difference between upper-tropospheric and lower-tropospheric velocity), and T the midtropospheric temperature. As for the midtropospheric upward vertical speed, it can be obtained using $w = \partial_x u + \partial_y v = Q - \varepsilon T$. The online supplementary material of Part I shows that the approximations made to obtain these equations (linearization and longwave approximation) are valid in the parameter range of interest, i.e., for synoptic- and planetary-scale circulations. It proves, in particular, that the linear equations approximately conserve energy.

On the right-hand side of Eq. (3), Q is the imposed heating, in the form

$$Q = F(x)D(y), \tag{4}$$

with

$$F(x) = \begin{cases} k\cos(kx) & \text{for} |x| < L_x, \\ 0 & \text{for} |x| > L_x, \end{cases} \text{ with } k = \frac{\pi}{2L_x} \tag{5}$$

and

$$D(y) = \frac{1}{L_y}\exp\left[-\frac{(y-y_0)^2}{4L_y^2}\right]. \tag{6}$$

This heating pattern is close to circular at its center for $L_x = 3L_y$. By construction; the horizontally integrated heating is kept constant: $[Q] = 4\sqrt{\pi}$. The equatorial case with $y_0 = 0$ is the focus of Part I, and the focus of this Part II is to analyze the solutions' sensitivity to y_0.

As shown in Part I, the method of solution is to use analytical solutions $(T^{(n)}, u^{(n)}, v^{(n)})$ to the Matsuno–Gill equations for diabatic heating in the form $Q^{(n)} = F(x)D_n(y)$, with D_n a parabolic cylinder function. D can be decomposed on the basis $\{D_n(y)\}_{n\in\mathbb{N}}$, and the solution for heating Q given by Eq. (4) can be written semianalytically as a series of the solutions $(T^{(n)}, u^{(n)}, v^{(n)})$ (see Part I for details).

In the off-equatorial case with $y_0 \neq 0$, D can be decomposed as follows:

$$D(y) = \sum_{n=0}^{\infty} a_n(L_y, y_0)D_n(y), \tag{7}$$

with

$$a_0 = \sqrt{\frac{2}{L_y^2+1}}\exp\left\{-\frac{y_0^2}{4\left(L_y^2+1\right)}\right\},$$

$$a_1 = \frac{y_0\, a_0}{L_y^2+1}, \tag{8}$$

and

$$a_n = \frac{y_0\, a_{n-1} + \left(L_y^2 - 1\right)a_{n-2}}{n\left(L_y^2+1\right)} \text{ for } n > 1.$$

Indeed, for $y_0 = 0$, this expression of a_n reduces to the expressions of a_{2n} and a_{2n+1} given in Part I [Eqs. (32) and (33)].

In practice, we approximate the infinite sum by a finite sum up to a value $n = m$ set by a convergence criterion (Cauchy 1821; see Part I).

b. Limits for heating with small zonal extent

Here, we explore the asymptotic solutions for $L_x \to 0$, focusing on the interval $-L_x \le x \le L_x$. Outside this interval, there is no simple expression for the infinite sums or integrals of exponentially decreasing modes that are solutions. Qualitatively, there is subsidence outside of $[-L_x, L_x]$ in both the β-plane and the f-plane cases.

Equations (38)–(41) in Part I give the asymptote in the limit $L_x \to 0$ for all latitudinal heating distribution D. In particular, we have in that limit $w \sim Q$, and, for the off-equatorial Gaussian heating distribution given by Eq. (6):

$$u: -2(1-\sin kx)\left[1 - \frac{y(y_0-y)}{4L_y^2}\right]D(y) + a_0 D_0(y). \tag{9}$$

In the limit $L_y \to 0$, the second term on the right-hand side is negligible in front of the first one.

3. Results

a. Temperature and wind response

We present here the features of the solutions in terms of temperature, surface winds, and midtropospheric vertical motion for a few cases with heating patterns of different horizontal extents centered away from the equator. In all these cases, we set $L_x = 3L_y$ so that isolines of heating are close to circular near its maximum. We have investigated cases with different ratios L_x/L_y and found that the sensitivity of the off-equatorial Gill circulation to the aspect ratio of the heating region is similar to the equatorial case discussed in Part I; in particular, the relative sensitivity of the global metrics of the circulation (intensities of the overturning circulation and the low-level westerly jet) to y_0 is almost independent of this ratio L_x/L_y. We show results for $L_x = 1.5L_y$ and $L_x = 6L_y$ in appendix A, and we focus on the case $L_x = 3L_y$ in the main text of this article.

Figure 1 depicts contours of temperature perturbation and surface velocity vectors forced by heating with meridional scale $L_y = 1$ (one equatorial radius of deformation, Figs. 1a,c) and $L_y = 1/2$ (Figs. 1b,d), centered at $y_0 = 1$ (Figs. 1a,b) and $y_0 = 2$ (Figs. 1c,d). Figure 2 shows the corresponding contours of midtropospheric vertical velocity together with contours of heating. Figures 1a, 1b, 2a, and 2b in Part I show the corresponding figures for the same heating pattern centered at the equator ($y_0 = 0$).

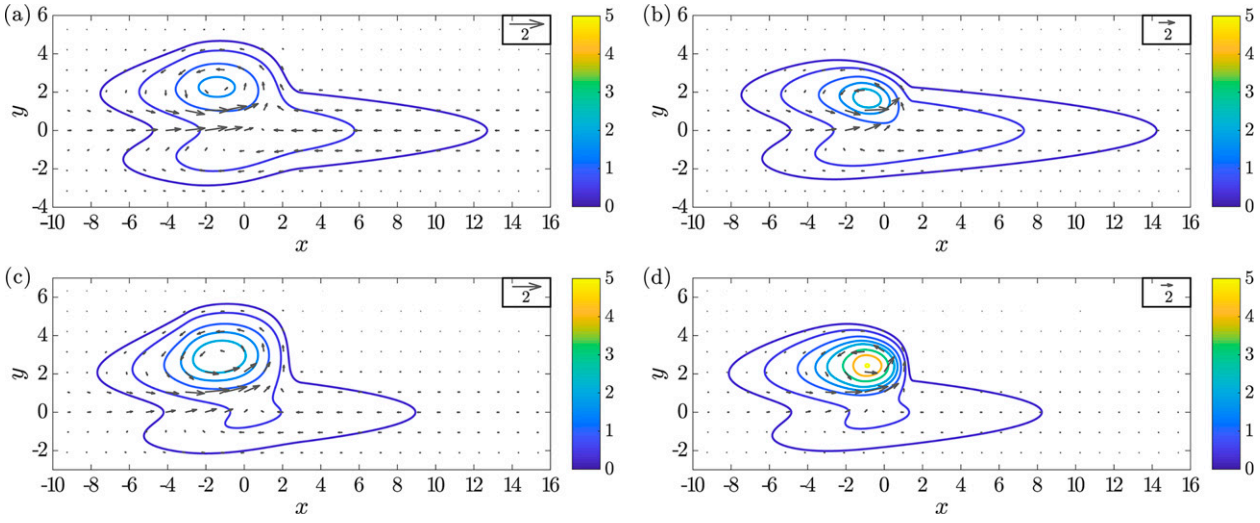

FIG. 1. Solutions for the Gill circulation: temperature response (contours) and low-level velocity (vectors) for (a) $(y_0, L_y) = (1, 1)$, (b) $(y_0, L_y) = (1, 1/2)$, (c) $(y_0, L_y) = (2, 1)$, and (d) $(y_0, L_y) = (2, 1/2)$; in all cases, $L_x = 3L_y$; temperature contours are at (0.25, 0.5, 1, 1.5, 2, 3, 4, 5).

The off-equatorial Gill circulation exhibits a strong rotational gyre, located poleward and westward of the heating center and a much weaker cyclonic gyre in the other hemisphere; it also exhibits Kelvin wave easterlies east of the heating region (Fig. 1). A low-level westerly jet develops between the equator and the heating center; it is similar to the observed monsoon jets. Compared to the equatorial case (Figs. 1a,b in Part I), the gyre next to the heating center and the low-level westerly jet equatorward of it are faster; the Kelvin wave easterlies and the gyre in the other hemisphere are weaker. Subsidence is preferentially west and poleward of the heating center, and more so for large y_0 and large horizontal extent of the heating (Fig. 2).

The sensitivity of the off-equatorial Gill circulation to the horizontal extent of the heating is similar to that of the equatorial circulation detailed in Part I. The smaller L_y, the faster

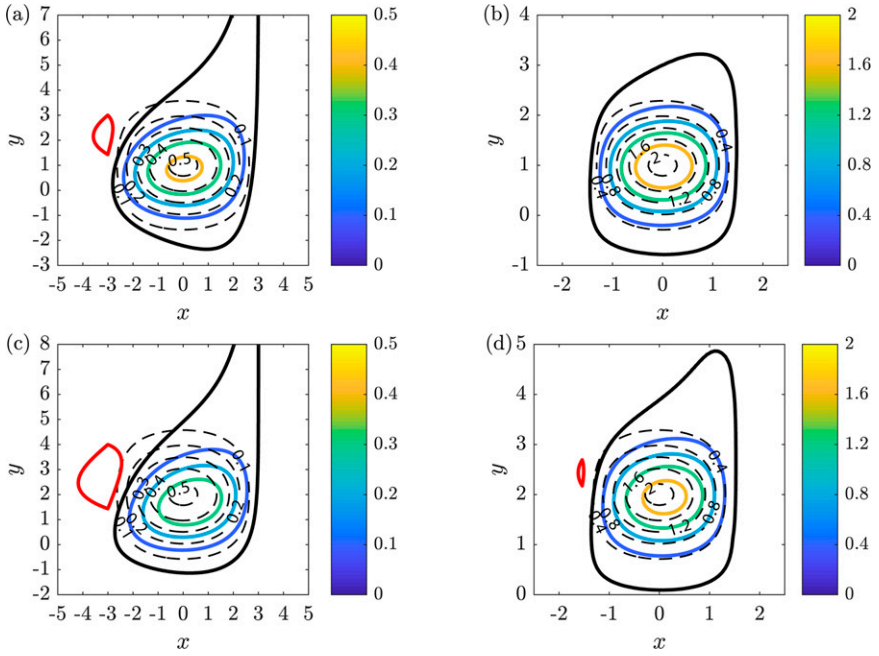

FIG. 2. Forcing and solution for the Gill circulation: diabatic heating (dashed contours) and midtropospheric vertical velocity (solid contours) for (a) $(y_0, L_y) = (1, 1)$, (b) $(y_0, L_y) = (1, 1/2)$, (c) $(y_0, L_y) = (2, 1)$, and (d) $(y_0, L_y) = (2, 1/2)$; in all cases, $L_x = 3L_y$. Contour spacing is 0.1 in (a) and (c) and 0.4 in (b) and (d), with black for $w = 0$ and red for $w < 0$.

the main gyre, the larger the temperature perturbations (Fig. 1), and the faster the ascending motions (Fig. 2).

As the latitude y_0 of the heating center is increased, the gyre near the heating moves poleward and becomes faster, and the temperature maximum increases, while the gyre in the other hemisphere and the equatorial, Kelvin-like easterlies weaken (Fig. 1). The latter can be attributed to the decrease of heating in the equatorial region. The ascending motion weakens and becomes more asymmetric with respect to the heating center (Fig. 2).

b. *Overturning circulation*

As in Part I, we study the intensity of the overturning circulation, because of its relevance to the coupling between dynamics and the hydrologic cycle. We define the intensity of the overturning circulation Γ as the upward vertical mass flux integrated over the horizontal [see Eq. (46) in Part I]; by mass conservation, it is the same as the downward vertical mass flux integrated over the horizontal. Γ is computed numerically on the basis of the semianalytical solutions.

Figure 3a shows the intensity Γ of the overturning circulation, as a function of y_0 and L_y. In all cases, the longitudinal extent of heating is still proportional to the latitudinal extent: $L_x = 3L_y$, so that L_y controls the horizontal extent of heating in both directions. For L_x, $L_y \to 0$, Γ is independent of y_0: $\Gamma \sim [Q]$, as established in section 2b). Γ decreases with L_y by up to 60% as in the equatorial case. For $y_0 = 0$, the sensitivity of Γ is that of the equatorial case studied in Part I (the decrease with L_y corresponds to the decrease along the diagonal of Fig. 3a in Part I). Γ also decreases slightly with y_0; Fig. 3b shows Γ as a percentage of its value in the equatorial case (for $y_0 = 0$), which confirms that Γ only decreases by up to 15% for y_0 going from 0 to 2.

This sensitivity is consistent with the effects of scale and rotation commented in section 3a of Part I. As shown by Eqs. (43) and (44) describing the f-plane case in section 2e of Part I, the vertical energy transport act as a diffusive effect of the direct, local temperature response Q/ε. It is less efficient for spatially smoother heating (i.e., larger scales) than for peaked heating (i.e., small scales), and it decreases if the heating center is displaced poleward because rotational effects become larger and a larger fraction of the energy input Q powers rotational winds to the expense of divergent motion. Equation (43) in Part I shows that, in the case of a damped inertio-gravity wave, the vertical motion scales with $(\varepsilon^2 + f^2)^{-1}$ and therefore decreases very significantly with increasing f. The vertical velocity (Fig. 2) and the sensitivity of Γ to y_0 suggest that this decrease is not as steep for the off-equatorial Gill circulation (on a β plane) as for the damped inertio-gravity wave (on an f plane).

Figure 2 suggests that most of the upward motion is limited to a region between $-L_x$ and L_x in longitude, with a meridional extent that scales with L_y. As in Part I, we find that Γ can be approximated by the integral Γ_* of w over the domain $([-L_x, L_x], [y_0 - 4L_y, y_0 + 4L_y])$, with the latitudinal bounds corresponding to twice the e-folding distance of D:

$$\Gamma_* = \int_{y^-}^{y^+} \int_{-L_x}^{L_x} w \, dx \, dy \approx \Gamma, \tag{10}$$

with $y^- = y_0 - 4L_y$ and $y^+ = y_0 + 4L_y$. Approximating Γ by Γ_* introduces an error that is small for most of the domain of (y_0, L_y) values considered here. It becomes significant only for unrealistically large horizontal heating regions. This approximation allows us to analyze the contribution of the different cylinder modes to the sensitivity of the overturning circulation; it can be decomposed in a series:

$$\Gamma_* = \sum_{n=0}^{\infty} \Gamma_*^{(n)} = \sum_{n=0}^{\infty} \Gamma_*^{(n,1)} + \Gamma_*^{(n,2)}, \tag{11}$$

with $\Gamma_*^{(n,1)}$ and $\Gamma_*^{(n,2)}$ the contributions of the first and second part of the response to the projection of heating Q onto the nth cylinder function D_n, i.e., a_n multiplied by the response to heating in the form $F(x)D_n(y)$.

$$\Gamma_*^{(n,i)} = a_n \int_{y^-}^{y^+} \int_{-L_x}^{L_x} w^{(n,i)} \, dx \, dy, \tag{12}$$

for $i = 1, 2$. Appendix B shows that we can write these contributions as

$$\Gamma_*^{(n,1)} = \gamma_n(L_x) f_n(y_0, L_y) + [1 - \gamma_{2n}(L_x)] g_{n,1}(y_0, L_y), \tag{13}$$

$$\Gamma_*^{(n,2)} = \gamma_{n+2}(L_x) f_n(y_0, L_y) + [1 - \gamma_{n+2}(L_x)] g_{n,2}(y_0, L_y), \tag{14}$$

with the variation in L_x given by the series of functions γ_n:

$$\begin{aligned} \gamma_0 &= \frac{1}{2} q_0^{(0)}(L_x) &&= \frac{1}{2} \frac{1 + e^{-2\varepsilon L_x}}{1 + \varepsilon^2 l_x^2}, \\ \gamma_1 &= 1, \\ \gamma_n &= \frac{1}{2} \frac{q_n^{(n)}(-L_x)}{n-1} = \frac{1}{2} q_n^{(n-2)}(-L_x) &&= \frac{1}{2} \frac{1 + e^{-2(2n-1)\varepsilon L_x}}{1 + (2n-1)^2 \varepsilon^2 l_x^2} \text{ for } n > 0, \end{aligned} \tag{15}$$

with $l_x = 1/k = 2L_y/\pi$; and the variation in y_0 and L_y given by

$$f_n = a_n(L_y) I_n \text{ with } I_n = \int_{y^-}^{y^+} D_n \, dy, \tag{16}$$

$$g_{n,1} = -\frac{2n}{2n-1} a_n(L_y) [D_{n-1}(y^+) - D_{n-1}(y^-)], \tag{17}$$

and

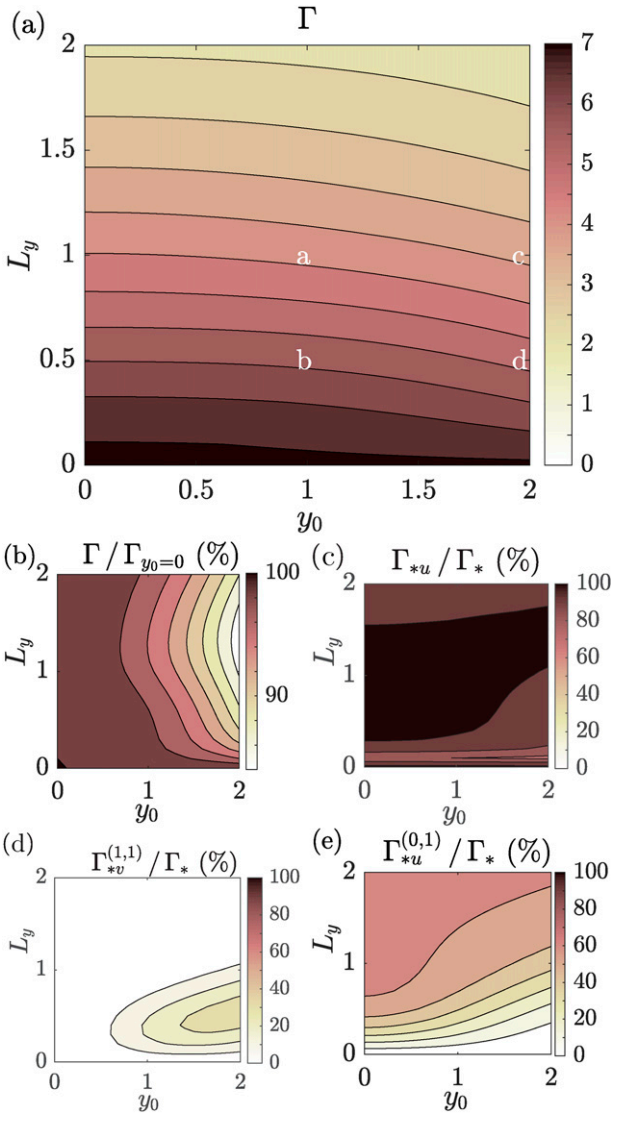

FIG. 3. (a) Intensity Γ of the overturning circulation for the β-plane case; the letters "a," "b," "c," and "d" indicate the cases shown in Figs. 1 and 2; (b) ratio of this intensity to that in the equatorial case ($y_0 = 0$); (c) contribution Γ_{*u} of the zonal flow to the approximated overturning circulation Γ_* (in % of Γ_*); (d) contribution $\Gamma^{(1,1)}_{*v}$ of the first component of the mode $n = 1$ (purely meridional flow) to the approximated overturning circulation Γ_* (in % of Γ_*); and (e) contribution $\Gamma^{(0,1)}_{*u}$ of the easterly flow to the approximated overturning circulation Γ_* (in % of Γ_*); in all cases, $L_x = 3L_y$.

$$g_{n,2} = \frac{2}{2n+3} a_n(L_y)\left[D_{n+1}(y^+) - D_{n+1}(y^-)\right]. \tag{18}$$

All these functions are consistent with the expressions obtained in Part I for $y_0 = 0$. We also have $I_1 = -2[D_0(y^+) - D_0(y^-)]$, which yields $g_{1,1} = f_1$. For $n \neq 1$, $\gamma_n \to 0$ for $L_x \to \infty$. As a result, $\Gamma^{(n,i)}_* \to g_{n,i}$ for all n and $i = 1, 2$ in that limit $L_x \to \infty$.

Since $\gamma_n(0) = 1$, $\Gamma^{(n,i)}_* = f_n$ for all n and $i = 1, 2$ in the limit $L_x \to 0$, and Γ_* in this limit can be expressed

$$\Gamma_*(0, L_y, y_0) = 2\int_{y^-}^{y^+} D \; dy = \mathrm{erf}(2)[Q]; \tag{19}$$

it is independent of y_0 and a good approximation of $\Gamma(0, L_y, y_0) = [Q]$ (as in the equatorial case).

Figure 4 shows some functions $\gamma_n(L_x)$ (for n even, these functions are also shown in Fig. 4a of Part I). All but γ_1 tend to zero for $L_x \to \infty$, and their decay is faster for larger n. For all $n \neq 1$, $\Gamma^{(n,i)}_*$ decreases from f_n for $L_x = 0$ to $g_{n,i}$ for $L_x \to \infty$ (with $i = 1, 2$). They converge faster toward their asymptotes for larger n; this is explained in Part I by the increasing effect of rotation on circulations forced by heating along cylinder functions D_n of increasing n, which have maxima increasingly far from the equator in regions of increasingly large Coriolis parameter. The increasing effect of rotation weakens the overturning circulation and increases the temperature perturbation. γ_1 is an exception: it is constant as a result of the zero temperature perturbation ($T^{(n,1)} = 0$). This means that the contribution $\Gamma^{(1,1)}_*$ will vary exclusively with L_y and y_0.

Figures 5–7 show the functions f_n, $g_{n,1}$, and $g_{n,2}$ for $n \leq 5$. The functions f_{2n}, $g_{2n,1}$, and $g_{2n,2}$ shown in Figs. 4c and 4d of Part I correspond to the axis $y_0 = 0$ in the first column of Figs. 5–7. For small y_0 and/or large L_y, the intensity of the circulation is dominated by the contributions from the projection of the heating on D_0 since f_0 is significantly larger than the other f_n, and γ_0 and γ_2 make the contributions of the two components $\Gamma^{(n,1)}_*$ and $\Gamma^{(n,2)}_*$ decay slowly toward $g_{0,1} = 0$ and $g_{0,2}$ (Figs. 4, 5a, and 7a); this is similar to the equatorial case. For larger y_0 and $L_y < 1$, the contributions for $n = 1$ become dominant instead, and more so for large L_x since γ_1 is constant (Figs. 4, 5b, and 7b). But the modes with larger n also contribute to the sensitivity of Γ to L_x, L_y, and y_0. Note that the limit of Γ_* for $L_x \to 0$ gives us a constraint on the sum of all f_n: $\sum_{n=0}^{\infty} f_n = \mathrm{erf}(2)[Q]$, independent of L_y and y_0. For $n > 1$, we can distinguish the domain $L_y \leq 1$ from the $L_y > 1$.

- For $L_y > 1$: for n odd, f_n, $g_{n,1}$, and $g_{n,2}$ decay rapidly toward zero as L_y increases (Figs. 5b,d,f, 6b,d, and 7b,d,f): this is a result of the decrease of a_n with increasing L_y and the fact that the D_n with n odd are odd functions of y, and compensations between the positive and negative segments of D_n contribute to reduce I_n. For n even, f_n are similar to the case $y_0 = 0$ (see Part I for details): they increase from zero at $L_y = 1$, reach a maximum and slowly decrease to zero for $L_y \to \infty$. The maximum value of f_n decreases with n and the value of L_y at which f_n reaches this maximum increases with n. As the sum of all f_n is constant, this means the decrease of f_0 with increasing L_y is compensated by f_n with increasingly large n. For $L_x > 0$, the contributions from these modes decrease like γ_n and γ_{n+2}, which decrease faster for larger n, and as a result the decrease of Γ_* with increasing L_x is faster for larger L_y, and creates a decrease of Γ_* with L_y for $L_x > 0$. To summarize, an increase in L_y results in larger projections of D onto cylinder functions D_n with larger n, which cause dynamical responses that are weaker in terms of divergent circulation due to the increasing influence of rotation. In this range of L_y, this decrease is very similar across

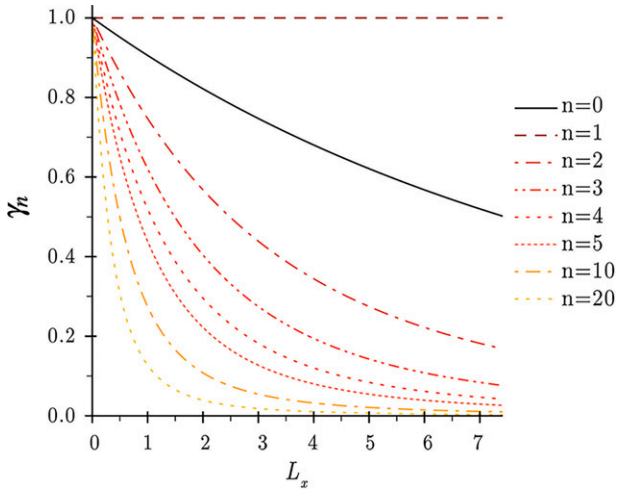

FIG. 4. Functions γ_n determining the sensitivity of the contribution $\Gamma_*^{(n,i)}$ to the longitudinal extent L_x of the diabatic heating for $n \leq 5$, $n = 10$, and $n = 20$.

the range of y_0 under consideration, so this sensitivity is similar to the equatorial case.

- For $L_y \leq 1$: the influence of modes with $n > 1$ is complex, with multiple compensations, and there is a stronger sensitivity to y_0. A few points can be made:
  - For all y_0, we can see that all $f_n \geq 0$ for small L_y, and it is zero if y_0 is a root of D_n. This is because the projection coefficient a_n is proportional to the cylinder function D_n for $L_y \to 0$:

$$a_n \approx \frac{\sqrt{2}}{n!} D_n(y_0),$$

and we have the following asymptotes:

$$I_n \sim 8 D_n(y_0) L_y \text{ and } f_n \sim \frac{8\sqrt{2}}{n!} D_n(y_0)^2 L_y \geq 0.$$

In the limit $L_x \to 0$, all modes contribute positively to Γ_* for small L_y. The asymptotes of functions $g_{n,1}$ and $g_{n,2}$ are proportional to $D_n(y_0)$, so they are zero for values of y_0 (among others) that also cancel f_n.

  - In the small-to-intermediate range of y_0, for $n > 1$, the integral I_n changes within an interval of L_y included in]0 1[because the sign of the function D_n is opposite to $D_n(0)$ for most of the interval $[y^- y^+]$. In terms of sensitivity to L_x and L_y, this causes large compensations between modes and between components of the modes in terms of sensitivity. For small y_0, it is very similar to the equatorial case (see Part I for details), with all $g_{n,1}$ and $g_{n,2}$ contributing positively to Γ_* in the limit $L_x \to \infty$; furthermore $g_{n,1} > f_n$ and $g_{n,2} < f_n$, which means that the contributions $\Gamma_*^{n,1}$ decrease the sensitivity of Γ_* to L_x while the contributions $\Gamma_*^{n,2}$ increase this sensitivity: there is a compensation between the contributions of the two components' gyres to the divergent circulation.

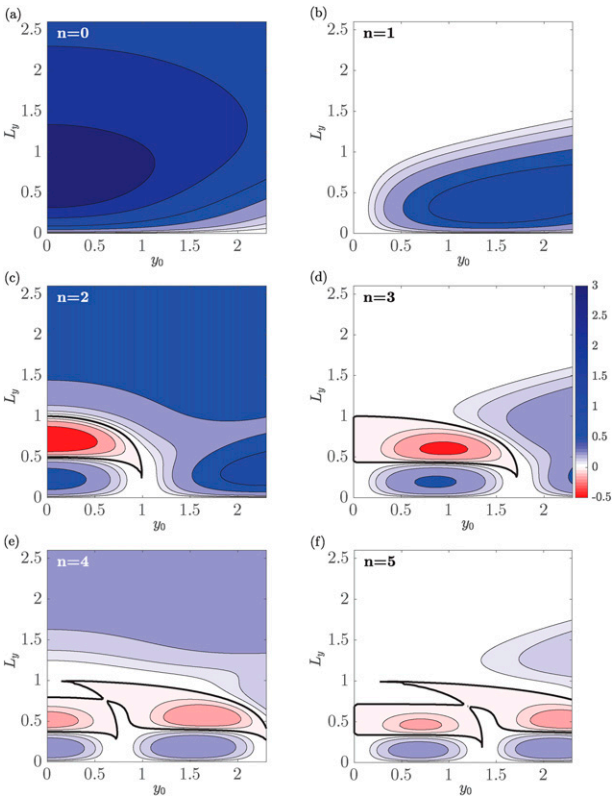

FIG. 5. Functions f_n determining the sensitivity of $\Gamma_*^{(n,i)}$ $(i = 1, 2)$ in the limit for $L_x = 0$ to the latitude of the y_0 of the diabatic heating and its latitudinal extent L_y, for $n \leq 1$.

  - For large y_0 (larger than the largest root of D_n), $D_n \sim y^n \exp - y^2/4$ is positive over the interval $[y^-, y^+]$, so its integral I_n is positive. We also have

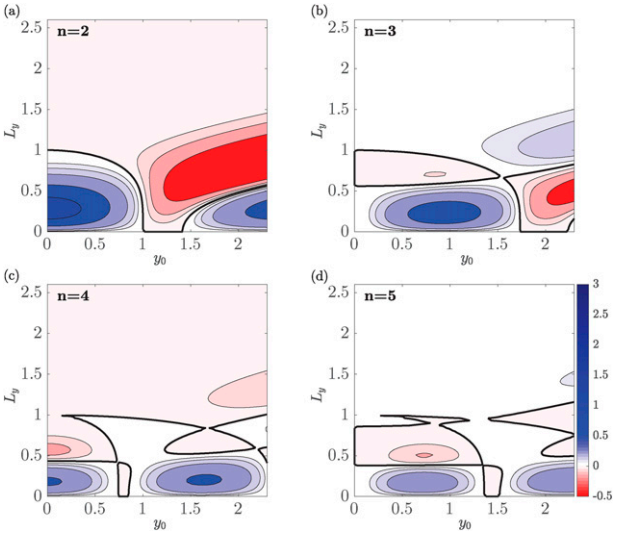

FIG. 6. Functions $g_{n,1}$ determining the sensitivity of $\Gamma_*^{(n,1)}$ in the limit for $L_x \to \infty$ to the latitude y_0 of the diabatic heating and its latitudinal extent L_y, for $n \leq 5$. $g_{0,1} = 0$ and $g_{1,1} = f_1$ are not shown.

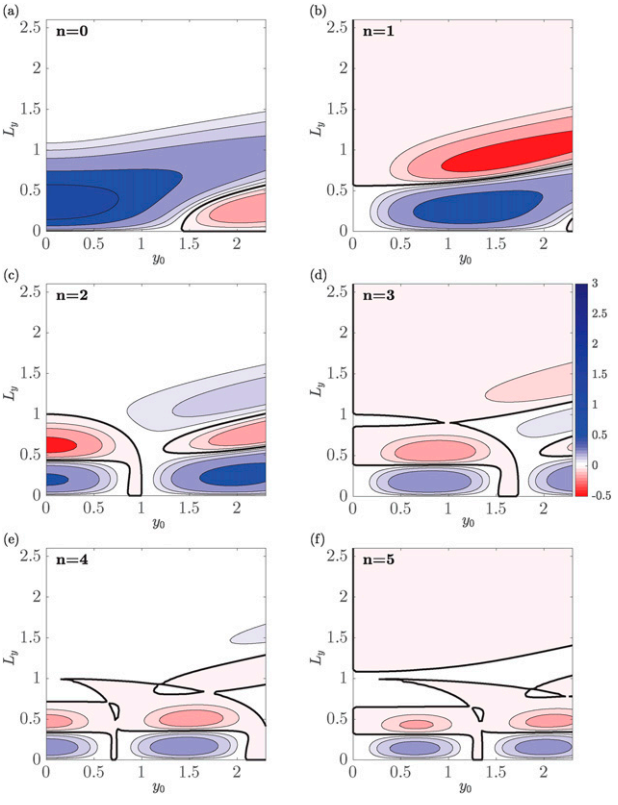

FIG. 7. Functions $g_{n,2}$ determining the sensitivity of $\Gamma_*^{(n,2)}$ in the limit for $L_x \to \infty$ to the latitude y_0 of the diabatic heating and its latitudinal extent L_y, for $n \leq 5$.

$$a_n \sim \frac{y_0^n}{n!\left(L_y^2+1\right)^n}\sqrt{\frac{2}{L_y^2+1}} > 0,$$

which yields $f_n = a_n I_n \geq 0$ for all L_y. I_n, and therefore f_n, increases for increasing small L_y (with $I_n = 0$ for $L_y = 0$) and a_n, and therefore f_n, tends to zero for large L_y. This asymptotic behavior is visible within the range of y_0 plotted in Fig. 5 for $n \leq 3$. For these large values of y_0, D projects increasingly on D_n of larger n (since a_n scales with y_0^n), and its sensitivity to the horizontal extent increases due to the larger influence of rotation on the dynamical response to heating along D_n with larger n. Despite these complex details, a few points appear clearly: (i) the two components of the cylinder modes $n = 0$ and $n = 1$ are the main contributors to Γ_*, because of large f_n, small $g_{n,2}$, and because γ_n decreases slowly (or not at all) with L_x; (ii) for mode $n = 0$, Kelvin wave and Rossby wave pattern both contribute to convergence in the heating region; (iii) for mode $n = 1$, the first component is exclusively divergent and contributes to a large part of the cross equatorial flow; (iv) for $n > 1$, the sensitivity of the first and second components $\Gamma_*^{(n,1)}$ and $\Gamma_*^{(n,2)}$ partially offset each other for small L_y, which explains the smaller influence of these modes.

Thanks to the continuity equation, we can also decompose Γ_* into the sum of a contribution from the meridional wind (v integrated over the boundary at $y = y^{\pm}$) and a contribution Γ_{*u} from the zonal wind (u integrated over the boundaries at $x = \pm L_x$). And each contribution $\Gamma_*^{(n,i)}$ can also be decomposed in the same way:

$$\Gamma_* = \Gamma_{*u} + \Gamma_{*v} \text{ and } \Gamma_*^{(n,i)} = \Gamma_{*u}^{(n,i)} + \Gamma_{*v}^{(n,i)}.$$

Because $u^{(0,1)}(-L_x) = 0$ and $u^{(n,i)}(L_x) = 0$ for all $n > 0$ or $i = 2$, the contribution from the zonal wind at the eastern border results exclusively from the damped Kelvin wave extending eastward from the heating pattern, while the contribution from the zonal wind at the western border results from a combination of damped Rossby waves. By integrating $u^{(n,i)}$ using Eqs. (17)–(24) in Part I, we can write

$$\Gamma_{*u}^{(n,1)} = \gamma_n(L_x)\left[f_n(y_0,L_y) - (2n-1)g_{n,1}(y_0,L_y)\right], \tag{20}$$

$$\Gamma_{*u}^{(n,2)} = \gamma_{n+2}(L_x)\left[f_n(y_0,L_y) + (2n+3)g_{n,2}(y_0,L_y)\right], \tag{21}$$

and we can obtain Γ_{*u} by summing over n. Note that $\Gamma_{*u}^{(1,1)} = 0$, as expected, since $f_1 = g_{1,1}$. Figure 3d shows that Γ_{*u} is the dominant contribution to Γ_*, above 90% for most of the parameter range under consideration, and even slightly above 100% for a significant parameter range, with little sensitivity to y_0. As in the equatorial case, the contribution Γ_{*v} from the meridional wind is small and can be negative, as shown in Fig. 3f, because of the compensation between the branches of the gyres in opposite directions. Within the contribution of the zonal wind, we can distinguish that of the damped Kelvin wave $\Gamma_{*u}^{(0,1)}$, which is also the contribution from the eastern boundary at $x = L_x$. Figure 3e shows that $\Gamma_{*u}^{(0,1)}$ is negligible for small L_y (and small $L_x = 3L_y$); this is consistent with the asymptote for $L_x \to 0$ [see Eq. (9), with $L_x = 3L_y$] in which the zonal wind is zero at $x = L_x$. $\Gamma_{*u}^{(0,1)}$ increases with increasing L_y, up to 60% of Γ_* for large L_y, larger than the contribution from the western boundary at $x = -L_x$. While the meridional contribution Γ_{*v} to Γ_* is small and in places negative (see Fig. 3f), the contribution $\Gamma_{*v}^{(1,1)}$ of the purely meridional flow for $n = 1$ is positive, and Fig. 3g shows that it can account for a significant fraction (up to 50%) of Γ_* for heating away from the equator for moderate values of L_y; in this case the combination of other contributions $\Gamma_{*v}^{(n,i)}$ essentially offsets this contribution $\Gamma_{*v}^{(1,1)}$.

c. *Equatorial westerly jet*

The β effect creates a low-level westerly jet between the heating center and the equator in the Gill circulation. If a coupling with surface thermodynamics is activated, this jet will decrease the surface turbulent heat fluxes if the background surface wind is easterly, for example in trade winds; it will increase the surface fluxes if the background wind is westerly, as in the equatorial the Indian Ocean or in monsoon jets. The resulting modulation of surface fluxes has been pointed out as a potential energy source for tropical intraseasonal variability (Bellon and Sobel 2008a,b; Sobel et al. 2008, 2010) and an important mechanism for their coupling with the surface ocean (Maloney and Sobel 2004; Bellon et al. 2008). In the

off-equatorial case, the westerly jet is not symmetric with respect to the central latitude of heating (see Fig. 1), it results mainly from the gyre near the heating center and reaches its maximum equatorward of the heating maximum. As can be seen in Fig. 1, as y_0 increases, the jet accelerates; as L_y decreases, the main gyre becomes smaller and faster, which also accelerates the low-level westerly jet. Appendix C details the characteristics of the jet for $L_y \to 0$.

The low-level westerly wind u_o at the heating center was studied in detail for the equatorial case in Part I; for the off-equatorial case, its sensitivity to the latitude y_0 of the heating center is small and its sensitivity to the horizontal extent of the heating L_x and L_y is similar to the equatorial case (see Fig. 5a in Part I). But u_o is not as relevant in the off-equatorial case as it is in the equatorial case: while in that case u_o is the maximum westerly wind on the y axis, in the off-equatorial case this maximum wind u_M is equatorward of the heating center. Figure 8a shows the sensitivity of this maximum wind: it increases with the latitude y_0 of the heating center, but mostly it increases with decreasing horizontal extent L_y, and tends toward infinity for $L_y \to 0$. Part I showed that, for $y_0 = 0$, $u_M = u_o \sim 2/L_y$ in that limit; appendix C shows that u_M diverges faster for $y_0 \neq 0$:

$$u_M \sim \frac{1}{\sqrt{2e}} \frac{y_0}{L_y^2}. \tag{22}$$

Figure 8b shows the latitudinal shift of this maximum low-level westerly wind along the y axis [$u_M = u(0, y_0 + y'_{u_M})$]. For large L_y (>1), the latitude of the wind maximum is mostly sensitive to y_0: the farther poleward the heating center, the farther the wind maximum from the heating center. For small L_y, the latitude of the wind maximum is mostly sensitive to L_y: it converges toward y_0 for very small L_y (appendix C shows that $y'_{u_M} \sim -\sqrt{2}L_y$ for $L_y \to 0$).

As in Part I, we also investigate the integrated intensity of the jet $U = -\int_{u<0} u(0,y)dy$, the longitudinal extent of the jet x_u along $y = y_0$, and characteristic latitudinal extent of the jet y_u along the y axis. Because the jet is not symmetric in latitude with respect to the heating center, the latitudinal extent y_u is the average between the poleward and equatorward extents:

$$y_u = \frac{1}{2}\left(y_u^+ - y_u^-\right), \text{ with } u\left(0, y_u^-\right) = u\left(0, y_u^+\right) = 0 \text{ and}$$
$$y_u^- < y_0 < y_u^+.$$

In addition, we introduce a measure of the asymmetry of the jet, the equatorward asymmetry index E_u, which measures how much more than half the jet is equatorward of the heating center ($E_u = 0$ corresponds to a jet symmetric about the latitude y_0, $E_u = 1$ to a jet entirely equatorward of the heating center):

$$E_u = 2\,\frac{y_0 - y_u^-}{y_u} - 1.$$

Figure 8c shows the sensitivity of the intensity U of the jet to y_0 and L_y. The sensitivity of U is similar to that of u_M, with an increase of U with increasing y_0, but mostly an increase of U with decreasing L_y. For $L_y \to 0$, U is finite if $y_0 = 0$ (see Part I), but if $y_0 \neq 0$, $U \sim y_0/L_y$ (see appendix C), which tends toward infinity for $L_y \to 0$. Figure 8e shows the latitudinal extent y_u of the jet along the y axis; it is not very sensitive to y_0 and scales roughly with the horizontal extent L_y of heating for moderate and large values of L_y. Appendix C shows that this linear scaling breaks down for $L_y \to 0$: $y_u \sim L_y\sqrt{-2\ln L_y}$. Compared to the equatorial case in which the scaling of the maximum wind $u_M = \sim 2/L_y$ and that of the latitudinal extent of the jet $y_u \sim 2L_y$ provide a finite upper bound for U, in the off-equatorial case there is no such upper bound: both the scaling of the wind maximum $u_M \sim y_0/(\sqrt{2e}L_y^2)$ and that of the jet's latitudinal extent $y_u \sim L_y\sqrt{-2\ln L_y}$ increase faster or decrease slower with decreasing L_y than in the equatorial case, and both effects explain the divergence of U for $L_y \to 0$. The scaling of y_u results from the slow convergence of the equatorward boundary y_u^- of the westerly jet toward y_0 for $L_y \to 0$, as can be seen from the asymmetry index E_u in Fig. 8f: $E_u \to 1$ for $y_0 \neq 0$ and $L_y \to 0$, which means that the jet extends exclusively equatorward of y_0 in this limit. The jet is

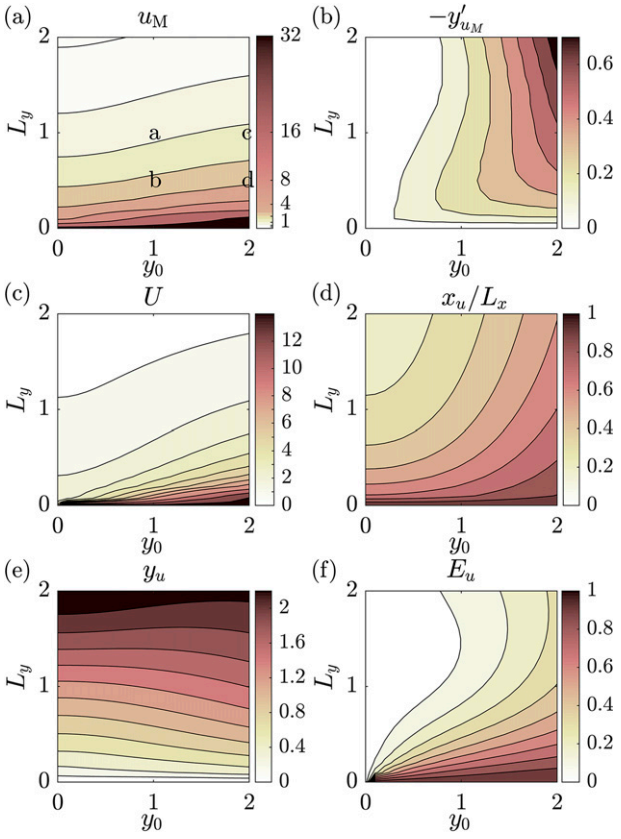

FIG. 8. Characteristics of the equatorial westerly jet in the Gill circulation: (a) maximum westerly zonal velocity u_M on the y axis; the letters "a," "b," and "c" indicate the cases shown in Figs. 1 and 2; (b) equatorward latitudinal shift $-y'_{u_M}$ of the maximum westerly zonal velocity; (c) intensity U of the jet; (d) zonal extent x_u of the jet normalized by L_x; (e) meridional extent y_u of the jet; (f) equatorward asymmetry index E_u of the jet.

symmetric about y_0 ($E_u = 0$) in the equatorial case ($y_0 = 0$), and the asymmetry of the jet increases with increasing y_0. It also decreases with increasing L_y for small L_y, but this sensitivity becomes nonlinear at larger L_y.

Finally, Fig. 8d shows the jet's eastward extent x_u along $y = y_0$, normalized by L_x. For small L_y (and small $L_x = 3L_y$), $x_u \approx L_x$, which means that the westerly jets extends longitudinally over the whole heating region at latitude y_0, irrespective of y_0 (see appendix C). The value of x_u/L_x decreases with L_y but more so in the equatorial case than in the off-equatorial case: for $y_0 = 2$, this decrease is twice smaller than for $y_0 = 0$.

In summary, compared to the equatorial case presented in Part I, the low-level westerly jet in the off-equatorial case

- has about the same latitudinal extent y_u except for small horizontal extents of heating for which y_u does tend toward zero for $L_y \to 0$, but more slowly than in the equatorial case;
- is about as fast at the heating center, but faster at its maximum wind speed, and causes a larger low-level eastward mass transport; these differences are markedly larger for L_x, $L_y \to 0$;
- is asymmetric with respect to the latitude y_0 of the heating center, extending farther equatorward than poleward, with its maximum wind speed equatorward of the heating center; for L_x, $L_y \to 0$, the jet is almost exclusively equatorward of the heating center; and
- extends farther eastward than in the equatorial case.

In terms of sensitivity to the horizontal extent of heating, the difference is significant in terms of the normalized longitudinal extent of the westerly jet (same limit for $L_y \to 0$, but less sensitivity to increasing L_y), and in terms of the maximum speed u_M and intensity U for small horizontal scales (larger scaling for $L_y \to 0$).

4. Summary and conclusions

In this article, we explore the scale sensitivity of the off-equatorial Gill circulation (Part I studies the equatorial case), keeping the horizontally integrated diabatic heating fixed in order to understand how the spatial spread of the diabatic heating influences the dynamical response of the tropical atmosphere. In our analysis, we focus on characteristics of this circulation likely to couple it with the energy cycle: intensity of the overturning circulation (linked to cloud moist processes) and characteristics of the low-level westerly flow (linked to turbulent surface heat fluxes).

We find that the intensity of the overturning circulation Γ decreases slightly with increasing latitude y_0 of the diabatic-heating center, except for very small horizontal extent of the heating for which it is independent of y_0 and the same as in the damped inertio-gravity wave. In other words, the sensitivity of Γ to the horizontal extent of the heating increases slightly with y_0. As argued in Part I from an energy perspective, if the heating center is displaced poleward, the effect of rotation is larger and the horizontal winds have a larger rotational component; the conversion of thermal energy to kinetic energy in rotational circulation is at the expense of the divergent circulation and reduces the overturning circulation.

The overturning circulation results mostly from the convergence of the zonal wind, with a large contribution of the Kelvin wave component for large-scale diabatic heating. The meridional contribution tends to be small and can be negative, despite a significant positive contribution of the meridional-only, $n = 1$, component for significantly off-equatorial diabatic heating. Also, the region of ascent is less and less collocated with the region of diabatic heating as the latitude of the heating increases. Overall, the sensitivity of the Gill circulation indicates that its coupling with the hydrologic cycle would create a weaker moisture-convergence feedback in the off-equatorial case compared to the equatorial case.

The low-level westerly jet intensifies as the diabatic heating is shifted poleward. At the same time the position of maximum wind respective to the heating center shifts equatorward. For small-scale heating, the jet extends entirely equatorward of the heating center, its latitudinal extent is very small, its maximum speed and the eastward low-level mass transport tend to infinity. This sensitivity of the low-level westerly jet is consistent with the monsoon low-level jet (Joseph and Raman 1966) being faster than the equatorial westerlies in the Indian Ocean during other seasons. It is also consistent with the large intraseasonal variability of this monsoon jet in response to the intraseasonal variability of convection (Joseph and Sijikumar 2004). The low-level westerly jet impacts turbulent surface fluxes, increasing them in westerlies and decreasing them in easterlies, and the intensity of this jet suggests a large impact. The combination of the seasonal monsoon jet and an intraseasonal westerly jet south of northward-propagating convective disturbances has been suggested as a growth mechanism for the boreal-summer monsoon intraseasonal oscillation (Bellon and Sobel 2008a,b; Sobel et al. 2010) and as a large component of its coupling with the ocean (Sengupta et al. 2001; Roxy and Tanimoto 2007; Bellon et al. 2008; Gao et al. 2019; among others). Our results suggest that, over mean westerlies, the wind-induced surface fluxes are larger and extend to a larger fraction of the heating region for small convective disturbances than for large convective disturbances, favoring the development of small disturbances. And these wind-induced surface fluxes are expected to increase with increasing latitude y_0 of the diabatic heating. But the influence of these surface fluxes on convective disturbances is not straightforward because of the location of the westerly low-level jet: the region of westerlies is increasingly asymmetric with respect to the heating center with decreasing horizontal extent of the diabatic heating, which favors equatorward propagation of a convective disturbance or slows poleward propagation in westerlies, additionally to enhancing the convective disturbance. The complex combination of sensitivities should have some bearings on the development, scale, and propagation of monsoon intraseasonal oscillation events worthy of further investigation.

The observed seasonal cycle in the tropics and observed boreal-summer monsoon intraseasonal oscillation provide multiple opportunities to evaluate whether the sensitivity to

scale and latitude of observed circulations responding to off-equatorial heating follows the sensitivity predicted by this study. This will be the topic of further work.

Acknowledgments. The authors acknowledge the support of the University of Auckland, and particularly financial support from its Faculty of Science in the form a Ph.D. fellowship and a grant from the Faculty Research Development Fund. G.B. is also supported by the Glavish-Buckley Lectureship.

APPENDIX A

Sensitivity to the Aspect Ratio L_x/L_y

This appendix investigates the sensitivity of the integrated metrics of the overturning circulation and the low-level westerly jet Γ and U to changes in the aspect ratio of the diabatic-heating region. Since isolines of heating are close to circular for $L_x = 3L_y$, which is the case discussed in the main text, we set $L_x = 3aL_y$ and document the sensitivity of our main results to parameter a. Figure A1 shows the ratio of the intensity Γ of the overturning circulation in the off-equatorial case to its intensity in the equatorial case ($y_0 = 0$) for different aspect ratios of the heating region: $a = 1/2$ (Fig. A1a) and $a = 2$ (Fig. A1b); the case $a = 1$ is shown in Fig. 3b. It appears that the sensitivity of Γ to the latitude of the heating varies little with the aspect ratio of the region of heating. In all cases, the intensity of the overturning circulation for $L_x \to 0$ is $\Gamma = [Q]$, independent of both L_y and y_0; for large L_x and L_y, the normalized decrease of Γ with increasing y_0 is similar in all cases. There is one difference in the scale for which this decrease with y_0 is fastest: while it is for $L_y \approx 1.3$ for $a = 1/2$, it is for a smaller $L_y \approx 0.5$ for $a = 2$.

Figure A2 shows that the sensitivity of the intensity of the westerly mass transport U exhibits a very similar sensitivity to the latitude y_0 of the heating center. The normalized increase of U with y_0 is essentially independent of a.

APPENDIX B

Contributions of the Cylinder Modes to Γ_*

By using the expressions of $w^{(n,i)}$ [Eq. (25) in Part I] combined with the expressions of $T^{(n,i)}$ [Eqs. (21)–(24) in Part I], we can write $\Gamma_*^{(n,i)}$ as

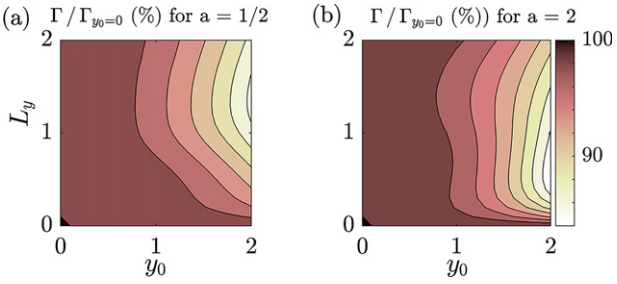

FIG. A1. Ratio of the intensity Γ of the overturning circulation in the off-equatorial case to its intensity in the equatorial case ($y_0 = 0$) for (a) $a = 1/2$ and (b) $a = 2$ ($L_x = 3aL_y$); the case $a = 1$ is shown in Fig. 3b.

$$\Gamma_*^{(n,1)} = a_n\left\{I_n - \frac{\varepsilon}{2}\int_{-L_x}^{L_x} q_n^{(n)}\,dx\,\left[I_n + nI_{(n-2)}\right]\right\}, \tag{B1}$$

$$\Gamma_*^{(n,2)} = a_n\left\{I_n - \frac{\varepsilon}{2}\int_{-L_x}^{L_x} q_{n+2}^{(n)}\,dx\,\left[I_{n+2} + (n+2)I_n\right]\right\}, \tag{B2}$$

for all n. We have used $\int_{-L_x}^{L_x} F\,dx = 2$ and introduced the notation $I_n = \int_{y-}^{y+} D_n\,dy$ for $n \geq 1$ and $I_{-1} = I_{-2} = 0$.The differential Eqs. (11) and (14) in Part I yield the following expressions for the integrals of the functions $q_{n(+2)}^{(n)}$:

$$\varepsilon\int_{-L_x}^{L_x} q_0^{(0)}\,dx = 2 - q_0^{(0)}(L_x), \tag{B3}$$

$$\varepsilon\int_{-L_x}^{L_x} q_1^{(1)}\,dx = 0, \tag{B4}$$

$$\varepsilon\int_{-L_x}^{L_x} q_n^{(n)}\,dx = \frac{1}{2n-1}\left[2n - 2 - q_n^{(n)}(-L_x)\right] \quad \text{for } n > 1, \tag{B5}$$

$$\varepsilon\int_{-L_x}^{L_x} q_{n+2}^{(n)}\,dx = \frac{1}{2n+3}\left[2 - q_{n+2}^{(n)}(-L_x)\right] \quad \text{for all } n, \tag{B6}$$

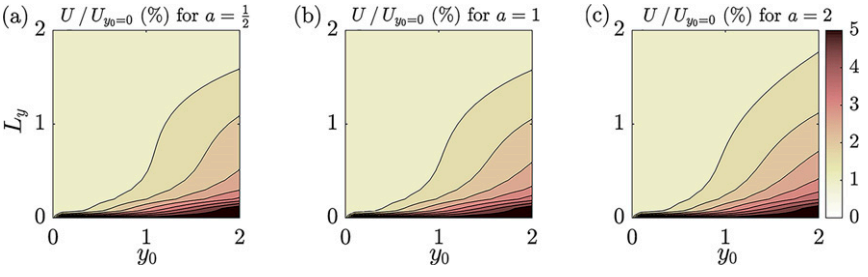

FIG A2. Ratio of the intensity U of the low-level westerly jet in the off-equatorial case to its intensity in the equatorial case ($y_0 = 0$) for (a) $L_x = 1.5L_y$, (b) $L_x = 3L_y$, and (c) $L_x = 6L_y$.

in which we have used $q_0^{(0)}(-L_x)=0$, $q_1^{(1)}=0$, $q_n^{(n)}(L_x)=0$ for $n>1$, and $q_{n+2}^{(n)}(L_x)=0$ for all n.

Equation (A6) in Part I yields

$$I_{n-2}=\frac{1}{n-1}\{I_n+2[D_{n-1}(y^+)-D_{n-1}(y^-)]\} \tag{B7}$$

and

$$I_{n+2}=(n+1)I_{2n}-2[D_{n+1}(y^+)-D_{n+1}(y^+)]. \tag{B8}$$

Using Eqs. (B3)–(B8), Eqs. (B1) and (B2) can be rewritten:

$$\Gamma_*^{(0,1)}=\frac{q_0^{(0)}(L_x)}{2}a_0I_0, \tag{B9}$$

$$\Gamma_*^{(1,1)}=a_1I_1, \tag{B10}$$

$$\Gamma_*^{(n,1)}=\frac{q_n^{(n)}(-L_x)}{2n-2}a_nI_n - \frac{2n}{2n-1}a_n[D_{n-1}(y^+)-D_{n-1}(y^-)]\left[1-\frac{q_n^{(n)}(-L_x)}{2n-2}\right] \quad \text{for } n>1, \tag{B11}$$

$$\Gamma_*^{(n,2)}=\frac{q_{n+2}^{(n)}(-L_x)}{2}a_nI_n + \frac{2}{2n+3}a_n[D_{n+1}(y^+)-D_{n+1}(y^-)]\left[1-\frac{q_{n+2}^{(n)}(-L_x)}{2}\right] \quad \text{for all } n. \tag{B12}$$

By replacing $q_n^{(n)}$ by its expressions [Eqs. (17)–(19) in Part I], and using $q_n^{(n)}=(n-1)q_n^{(n-2)}$, $\Gamma_*^{(n,i)}$ can be written as in Eqs. (13) and (14).

The contribution $\Gamma_{*u}^{(n,i)}$ to $\Gamma_*^{(n,i)}$ from the zonal flow is simply the integral of the zonal velocity $u^{(n,i)}$ over the zonal boundary of the rectangle $(2L_x, 8L_y)$ where it is not zero, multiplied by $\pm a_n$. Using the expressions of $u^{(n,i)}$ [Eqs. (17)–(24) in Part I], it can be written as

$$\Gamma_{*u}^{(0,1)}=\frac{a_0}{2}q_0^{(0)}(L_x)I_0=\Gamma_*^{(0,1)}, \tag{B13}$$

$$\Gamma_{*u}^{(1,1)}=0, \tag{B14}$$

$$\Gamma_{*u}^{(n,1)}=-\frac{a_n}{2}q_n^{(n)}(-L_x)[I_n-nI_{n-2}] \text{ for } n>1, \tag{B15}$$

$$\Gamma_{*u}^{(n,2)}=-\frac{a_n}{2}q_{n+2}^{(n)}(-L_x)[I_{n+2}-(n+2)I_n] \text{ for all } n. \tag{B16}$$

The last two can be simplified into [using Eq. (A6) in Part I]

$$\Gamma_{*u}^{(n,1)}=\frac{q_n^{(n)}(-L_x)}{2n-2}a_n\{I_n+2n[D_{n-1}(y^+)-D_{n-1}(y^-)]\} \quad \text{for } n>1, \tag{B17}$$

$$\Gamma_{*u}^{(n,2)}=\frac{q_{n+2}^{(n)}(-L_x)}{2}a_n\{I_n+2[D_{n+1}(y^+)-D_{n+1}(y^-)]\} \quad \text{for all } n. \tag{B18}$$

By replacing $q_n^{(n)}$ by its expression from Eqs. (17)–(19) in Part I, and using $q_n^{(n)}=(n-1)q_n^{(n-2)}$, $\Gamma_{*u}^{(n,i)}$ can be written as in Eqs. (20) and (21).

APPENDIX C

Characteristics of the Jet for $L_y \to 0$

In this appendix, we focus on the limit of the solution for L_y (and L_x) $\to 0$ in the off-equatorial case ($y_0 \neq 0$). From Eq. (9), which gives the expression of the zonal baroclinic wind field for $L_x \to 0$, it is clear that along $y = y_0$, the zonal wind is negative (westerly in the low-troposphere) for $x \leq x_u$, with

$$x_u \sim \frac{1}{k}\arcsin\left(1-\frac{a_0}{2}e^{-y_0^2/4}L_y\right) \to L_x \text{ for } L_y \to 0, \tag{C1}$$

since $a_0 \to \sqrt{2}\exp\left(-y_0^2/4\right)$ and $k = \pi/2Lx$.

Along the y axis, the baroclinic zonal wind can be written:

$$u(0,y)=-2\left[1-\frac{y(y-y_0)}{4{L_y}^2}\right]D(y)+a_0D_0(y); \tag{C2}$$

for $L_y \to 0$, it is westerly around the heating center ($u_o < 0$) and it is easterly for $y = 0$. There is no straightforward solution for the latitude of sign change or maximum of $u(0, y)$. But we can see that for small L_y the westerly jet becomes narrow and close to y_0, so we can look for solutions in the form of a asymptotic development:

$$y=y_0+\sum_{n=1}^{\infty}b_nL_y^n. \tag{C3}$$

For $u(0, y) = 0$, this yields one solution:

$$y_u^+ \sim y_0+\frac{4}{y_0}L_y^2, \tag{C4}$$

and it is unsuccessful to determine y_u^- [because $y(y - y_0) < 0$ in the range of y of interest, and the first parenthesis on the right-hand side in Eq. (C2) is always larger than 1]. By a careful study of the scalings of the different terms in Eq. (C2), we can find the following asymptotic solution:

$$y_u^- \sim y_0-2\sqrt{2}L_y\left\{\mathscr{y}+\frac{1}{4\mathscr{y}}\left[\ln(\mathscr{y}\,y_0)+\frac{y_0^2}{2}\right]\right\}, \tag{C5}$$

with $\mathscr{y} = \sqrt{-\ln L_y}$.

For $L_y \to 0$, we can obtain an expression for U using Eq. (9) to integrate $u(0, y)$ by parts over the interval $[y_u^- \; y_u^+]$:

$$U = y_u{}^+ D\left(y_u^+\right) - y_u{}^- D(y_u^-) + \sqrt{\pi}\left[\mathrm{erf}\left(\frac{y_u^+ - y_0}{2L_y}\right) - \mathrm{erf}\left(\frac{y_u^- - y_0}{2L_y}\right)\right] + a_0\sqrt{\pi}\left[\mathrm{erf}\left(\frac{y_u^+}{2}\right) - \mathrm{erf}\left(\frac{y_u^-}{2}\right)\right], \tag{C6}$$

and taking the limit for $L_y \to 0$ (using the approximations of y_u^+ and y_u^- above), we get

$$U \sim \frac{y_0}{L_y}. \tag{C7}$$

As for the maximum westerly wind, it is located at $y = y_{u_M}$ where

$$0 = \frac{du(0,y)}{dy} = \frac{1}{2L_y^2}\left[3y' + y\left(1 - \frac{y'^2}{2L_y^2}\right)\right]D(y) - \frac{a_0}{2}yD_0(y), \tag{C8}$$

in which we used $y' = y - y_0$ for simplicity.

Looking for an asymptotic expansion following Eq. (C3) for y_{u_M}, we find

$$y_{u_M} \sim y_0 - \sqrt{2}L_y \tag{C9}$$

and the expression of u_M in Eq. (22).

REFERENCES

Bellon, G., and J. Srinivasan, 2006: Comments on "Structures and mechanisms of the northward propagating boreal summer intraseasonal oscillation." *J. Climate*, **19**, 4738–4743, https://doi.org/10.1175/JCLI3861.1.

——, and A. H. Sobel, 2008a: Instability of the axisymmetric monsoon flow and intraseasonal oscillation. *J. Geophys. Res.*, **113**, D07108, https://doi.org/10.1029/2007JD009291.

——, and ——, 2008b: Poleward-propagating intraseasonal monsoon disturbances in an intermediate-complexity axisymmetric model. *J. Atmos. Sci.*, **65**, 470–489, https://doi.org/10.1175/2007JAS2339.1.

——, ——, and J. Vialard, 2008: Ocean–atmosphere coupling in the monsoon intraseasonal oscillation: A simple model study. *J. Climate*, **21**, 5254–5270, https://doi.org/10.1175/2008JCLI2305.1.

Boos, W. R., and Z. Kuang, 2010: Mechanisms of poleward propagating, intraseasonal convective anomalies in cloud system–resolving models. *J. Atmos. Sci.*, **67**, 3673–3691, https://doi.org/10.1175/2010JAS3515.1.

Cauchy, A. L. B., 1821: *Cours d'analyse de l'École Royale Polytechnique: Analyse algébrique*. Vol. 1. Debure frères, 576 pp.

Gao, Y., N. P. Klingaman, C. A. DeMott, and P.-C. Hsu, 2019: Diagnosing ocean feedbacks to the BSISO: SST-modulated surface fluxes and the moist static energy budget. *J. Geophys. Res. Atmos.*, **124**, 146–170, https://doi.org/10.1029/2018JD029303.

Gill, A. E., 1980: Some simple solutions for heat-induced tropical circulation. *Quart. J. Roy. Meteor. Soc.*, **106**, 447–462, https://doi.org/10.1002/qj.49710644905.

Goswami, B. N., 2005: South Asian monsoon. *Intraseasonal Variability in the Atmosphere-Ocean Climate System*, W. K. M. Lau and D. E. Waliser, Eds., Springer, 19–61.

Jiang, X., T. Li, and B. Wang, 2004: Structures and mechanisms of the northward propagating boreal summer intraseasonal oscillation. *J. Climate*, **17**, 1022–1039, https://doi.org/10.1175/1520-0442(2004)017<1022:SAMOTN>2.0.CO;2.

Joseph, P. V., and P. L. Raman, 1966: Existence of low level westerly jet stream over peninsular India during July. *Ind. J. Meteor. Geophys.*, **17**, 407–410.

——, and S. Sijikumar, 2004: Intraseasonal variability of the low-level jet stream of the Asian summer monsoon. *J. Climate*, **17**, 1449–1458, https://doi.org/10.1175/1520-0442(2004)017<1449:IVOTLJ>2.0.CO;2.

Kang, I.-S., D. Kim, and J.-S. Kug, 2010: Mechanism for northward propagation of boreal summer intraseasonal oscillation: Convective momentum transport. *Geophys. Res. Lett.*, **37**, L24804, https://doi.org/10.1029/2010GL045072.

Maloney, E., and A. H. Sobel, 2004: Surface fluxes and ocean coupling in the tropical intraseasonal oscillation. *J. Climate*, **17**, 4368–4386, https://doi.org/10.1175/JCLI-3212.1.

Matsuno, T., 1966: Quasi-geostrophic motions in the equatorial area. *J. Meteor. Soc. Japan*, **44**, 25–43, https://doi.org/10.2151/jmsj1965.44.1_25.

Ramage, C. S., 1971: *Monsoon Meteorology*. Academic Press, 296 pp.

Reboredo, B., and G. Bellon, 2021: Scale sensitivity of the Gill circulation. Part I: Equatorial case. *J. Atmos. Sci.*, https://doi.org/10.1175/JAS-D-21-0067.1, **79**, 3–17.

Roxy, M., and Y. Tanimoto, 2007: Role of SST over the Indian Ocean in influencing the intraseasonal variability of the Indian summer monsoon. *J. Meteor. Soc. Japan*, **85**, 349–358, https://doi.org/10.2151/jmsj.85.349.

Sengupta, D., B. N. Goswami, and R. Senan, 2001: Coherent intraseasonal oscillations of ocean and atmosphere during the Asian summer monsoon. *Geophys. Res. Lett.*, **28**, 4127–4130, https://doi.org/10.1029/2001GL013587.

Sharmila, S., and Coauthors, 2013: Role of ocean–atmosphere interaction on northward propagation of Indian summer monsoon intra-seasonal oscillations (MISO). *Climate Dyn.*, **41**, 1651–1669, https://doi.org/10.1007/s00382-013-1854-1.

Sobel, A. H., E. D. Maloney, G. Bellon, and D. M. Frierson, 2008: The role of surface heat fluxes in tropical intraseasonal oscillations. *Nat. Geosci.*, **1**, 653–657, https://doi.org/10.1038/ngeo312.

——, ——, ——, and ——, 2010: Surface fluxes and tropical intraseasonal variability: A reassessment. *J. Adv. Model. Earth Syst.*, **2**, 2, https://doi.org/10.3894/JAMES.2010.2.2.

Webster, P. J., 1972: Response of the tropical atmosphere to local, steady forcing. *Mon. Wea. Rev.*, **100**, 518–541, https://doi.org/10.1175/1520-0493(1972)100<0518:ROTTAT>2.3.CO;2.

Wu, G. X., Y. Liu, X. Zhu, W. Li, R. Ren, A. Duan, and X. Liang, 2009: Multi-scale forcing and the formation of subtropical desert and monsoon. *Ann. Geophys.*, **27**, 3631–3644, https://doi.org/10.5194/angeo-27-3631-2009.